Journal of Alloys and Compounds 580 (2013) 435–441

Contents lists available at SciVerse ScienceDirect

Journal of Alloys and Compounds

journal homepage: www.elsevier.com/locate/jalcom

Valence fluctuation in $CeMo_2Si_2C$

U.B. Paramanik [a], Anupam [a], U. Burkhardt [b], R. Prasad [a], C. Geibel [b], Z. Hossain [a,*]

[a] Department of Physics, Indian Institute of Technology, Kanpur 208 016, India
[b] Max-Planck Institute for Chemical Physics of Solids, 01187 Dresden, Germany

ARTICLE INFO

Article history:
Received 14 March 2013
Received in revised form 22 May 2013
Accepted 24 May 2013
Available online 5 June 2013

Keywords:
Rare earth alloys and compounds
Valence fluctuations
Magnetic measurements
Heat capacity
X-ray absorption spectroscopy
Electronic structure

ABSTRACT

We report on the valence fluctuation of Ce in $CeMo_2Si_2C$ as studied by means of magnetic susceptibility $\chi(T)$, specific heat $C(T)$, electrical resistivity $\rho(T)$ and X-ray absorption spectroscopy. Powder X-ray diffraction revealed that $CeMo_2Si_2C$ crystallizes in $CeCr_2Si_2C$-type layered tetragonal crystal structure (space group *P4/mmm*). The unit cell volume of $CeMo_2Si_2C$ deviates from the expected lanthanide contraction, indicating non-trivalent state of Ce ions in this compound. The observed weak temperature dependence of the magnetic susceptibility and its low value indicate that Ce ions are in valence fluctuating state. The formal L_{III} Ce valence in $CeMo_2Si_2C\langle\tilde{v}\rangle = 3.14$ as determined from X-ray absorption spectroscopy measurement is well below the value $\langle\tilde{v}\rangle \simeq 3.4$ in tetravalent Ce compound CeO_2. The temperature dependence of specific heat does not show any anomaly down to 1.8 K which rules out any magnetic ordering in the system. The Sommerfeld coefficient obtained from the specific heat data is $\gamma = 23.4$ mJ/mol K^2. The electrical resistivity follows the T^2 behavior in the low temperature range below 35 K confirming a Fermi liquid behavior. Accordingly both the Kadowaki Woods ratio A/γ^2 and the Sommerfeld Wilson ratio $\chi(0)/\gamma$ are in the range expected for Fermi-liquid systems. In order to get some information on the electronic states, we calculated the band structure within the density functional theory, even-though this approach is not able to treat 4*f* electrons accurately. The non-*f* electron states crossing the Fermi level have mostly Mo 4*d* character. They provide the states with which the 4*f* sates are strongly hybridized, leading to the intermediate valent state.

1. Introduction

The Ce-based intermetallic compounds have attracted tremendous attention with interesting phenomena such as valence fluctuations, heavy fermion behavior, quantum criticality, unconventional superconductivity and Kondo effect [1–4]. These anomalous properties arise due to the hybridization between the localized (4*f*) electrons and conduction electrons. Usually, the competition between Ruderman–Kittel–Kasuya–Yosida (RKKY) and Kondo interactions determines the ground state of these compounds. While the RKKY interaction favors a long-range magnetic order, the Kondo interactions have a tendency to screen the magnetic moments which lead to a non-magnetic ground state [5,6]. The result of these two interactions is summarized in the Doniach phase diagram [5]. A quantum critical point exists in the regime where the strength of RKKY and Kondo interactions are comparable. Quantum criticality in heavy fermion systems is one of the hot topics in condensed matter physics. In Ce-based compounds, quantum criticality and associated unusual physical properties such as the non-Fermi liquid behavior are found near the magnetic non-magnetic crossover, where the Ce valency is very close to 3+. Usually one uses a tuning parameter such as pressure, doping or magnetic field to tune the electronic ground state of the system close to quantum critical point. Many Ce-based compounds exhibit magnetically mediated unconventional superconductivity in the quantum critical regime. Despite the first such superconductor, $CeCu_2Si_2$ [7], was discovered 35 years ago, many fundamental questions have yet not been settled and there is still an intensive research going on these superconductors. Pressure experiments on pure and Ge-doped $CeCu_2Si_2$ revealed two superconducting domes, one at lower pressure attributed to the magnetic quantum critical point and the other one at a higher pressure which could be related to valence fluctuation [8,9]. In contrast, unconventional superconductivity was not found in Yb-compounds near a magnetic quantum critical point, even though there are examples of Yb-compounds showing quantum criticality. $YbAlB_4$ is the only compound showing superconductivity which is proposed to be connected with critical valence fluctuations [10–12]. This provided additional incentive for the investigations of valence fluctuation phenomenon.

In our search for new valence fluctuating compound that may show quantum criticality similar to that of $YbAlB_4$, we have synthesized and investigated the physical properties of $CeMo_2Si_2C$.

* Corresponding author. Tel.: +91 51 2679 7464.
E-mail address: zakir@iitk.ac.in (Z. Hossain).

0925-8388/$ - see front matter © 2013 Elsevier B.V. All rights reserved.
http://dx.doi.org/10.1016/j.jallcom.2013.05.169

To the best of our knowledge, there is no report in the literature on the layered intermetallic compound $CeMo_2Si_2C$. The structurally homologous compound, $PrMo_2Si_2C$ [13] has been reported to form in $CeCr_2Si_2C$-type ("filled" $CeMg_2Si_2$-type) tetragonal crystal structure (space group *P4/mmm*). The magnetic measurements on $PrMo_2Si_2C$ have suggested a trivalent state of Pr in this compound. RCr_2Si_2C (R = Y, La-Sm, Gd-Er), an isoelectronic structural homologue series of $CeMo_2Si_2C$, has been reported to exhibit ferromagnetic ordering of rare earth ions [14] but intermediate valence for R = Ce [15,16]. We present the structural and physical properties of $CeMo_2Si_2C$, viz., X-ray diffraction (XRD), dc magnetic susceptibility, electrical resistivity, specific heat and X-ray absorption spectroscopy (XAS) and discuss the results in the context of the calculated electronic structure. From our measurements, we show that Ce ions are in a valence fluctuating state in this compound.

2. Methods

2.1. Experiment

Polycrystalline sample of $CeMo_2Si_2C$ has been prepared by the standard arc melting technique on a water cooled copper hearth. Since the melting point of Molybdenum element is very high, therefore, we first arc melted Si and Mo together in the stoichiometric ratio. Then the as-obtained pellet was arc melted with carbon and subsequently with cerium. All the constituent elements were of high purity (99.9% and above). The samples were flipped after each melting and were melted several times to ensure homogeneity. The arc melted button was sealed in the Ta crucible and annealed in a vacuum furnace at 1500 °C for five days. The phase purity of the sample was checked by powder X-ray diffraction using Cu Kα radiation and scanning electron micrograph (SEM). Energy dispersive X-ray (EDX) analysis was used to check the stoichiometry of the sample. Electrical resistivity measurements were carried out using conventional four probe technique in the temperature range 2–300 K in a physical property measurement system (PPMS, Quantum design). A commercial superconducting quantum interference device (SQUID) magnetometer (MPMS, Quantum design) was used for magnetic measurements. The specific heat was measured by relaxation method in a physical property measurement system (PPMS, Quantum design). The absorption spectra of $CeMo_2Si_2C$ at the Ce-L_{III} edge (E = 5723 eV) have been recorded in transmission mode at the EXAFS beam line A1 of the Hamburg synchrotron radiation facility (HASYLAB at DESY) using the Si(111) double crystal monochromator. The absorption behavior has been determined in the energy range 5450–6200 eV with a minimal step size of $\Delta E = 0.2$ eV close to the absorption edge, e.g. 5723 ± 25 eV. The powdered sample with particle size smaller than 20 μm was distributed on self adhesive Kapton foil. Multi-layers of 4 foils corresponding to 8 mg/cm^2 resulted an absorption edge step of $\Delta\mu = 0.5$ which represents the difference of the low and high energy background functions at the absorption edge. Evaluation of spectra, energy calibration and normalization have been performed with the Athena modul of the Horae software package [17]. The simultaneously measured reference spectra of the Ce^{3+} compound $CePO_4$ was used for energy calibration and was measured together with the CeO_2 reference material with a dominant Ce^{4+} contribution.

2.2. Method of calculation

We have performed the density-functional band structure calculations using two full potential codes: local orbital minimum basis band structure scheme (FPLO) [18] and full-potential linearized augmented plane wave (FLAPW) method implemented in WIEN2K code [19]. Perdew–Burke–Ernzerhof (PBE) form of the generalized gradient approximation (GGA) was employed for the exchange correlation potential [20]. Additionally, to account for the strong Coulomb repulsion within the Ce (4*f*) orbitals a typical value of the Coulomb energy U = 6 eV has been chosen for the GGA + U calculations [21,22]. The calculations were performed using the experimentally obtained lattice parameters of $CeMo_2Si_2C$ where the full-lattice optimizations were done using Rietveld refined atomic coordinates.

3. Results and discussion

3.1. Experiment

Fig. 1 shows the XRD pattern of $CeMo_2Si_2C$ together with the structural Rietveld refinement profile for the $CeCr_2Si_2C$-type layered tetragonal crystal structure (space group *P4/mmm*). Powder X-ray diffraction data were collected on the crushed sample and analyzed by Rietveld refinement using `FullProf` software [23].

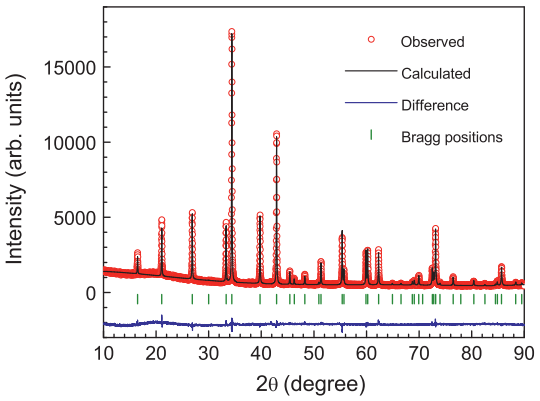

Fig. 1. The powder X-ray diffraction pattern of $CeMo_2Si_2C$ recorded at room temperature. The solid line through the experimental points is the Rietveld refinement profile calculated for the $CeCr_2Si_2C$-type layered tetragonal crystal structure (space group *P4/mmm*). The short vertical bars indicate the Bragg peak positions. The lowermost curve represents the difference between the experimental and model results.

The obtained lattice parameters for $CeMo_2Si_2C$ are a = 4.213(1) Å, and c = 5.376(1) Å which are smaller than the values reported for homologous $PrMo_2Si_2C$ (a = 4.214 Å and c = 5.409 Å) [13]. That means $CeMo_2Si_2C$ unit cell volume does not follow the usual lanthanide contraction which is a first indication for a valence fluctuating Ce states.

The crystallographic parameters obtained from the least square refinement of XRD data are listed in Table 1 and Table 2. The XRD and SEM reveal the single phase nature of the sample. The EDX composition analysis confirmed the desired stoichiometry of $CeMo_2Si_2C$. The $CeCr_2$ Si_2C-type primitive tetragonal crystal structure of $CeMo_2Si_2C$ is presented schematically in Fig. 2. This structure is different from the very common tetragonal $ThCr_2$)Si_2-type structure: an additional carbon atom sharing the same edge with Mo forms a layer of MoC. The loss of the body centering results in the c/a ratio 1.27 which is almost half of usually observed ratio of about 2.5 in the $ThCr_2Si_2$-type structure. The value of the lattice parameter c in this structure suggests a covalent bonding between the Ce–C along [0 0 1] direction [15]. The Ce atoms lie at the midpoint of the c-axis of the unit cell and there is no direct bonding between them.

The temperature dependence of magnetic susceptibility $\chi(T)$ of $CeMo_2Si_2C$ measured under an applied magnetic field of H = 5 T is shown in Fig. 3. The very low value of susceptibility and its weak temperature dependence down to 100 K clearly indicate that Ce ions are in valence fluctuating state. Similar shape of susceptibility

Table 1
Crystallographic parameters obtained from the Rietveld refinement of powder X-ray diffraction data for $CeMo_2Si_2C$.

Structure				$CeCr_2Si_2C$-type tetragonal	
Space group				*P4/mmm*	
Lattice parameters					
a (Å)				4.213(1)	
c (Å)				5.376(1)	
V_{cell}(Å^3)				95.42(1)	
Refinement quality					
χ^2				1.36	
R_P				3.15	
R_{WP}				4.08	
Refined atomic coordinates					
Atom	Wyckoff	x	y	z	B
Ce	1*b*	0.0000	0.0000	0.5000	0.10784
Mo	2*f*	0.0000	0.5000	0.0000	0.07548
Si	2*h*	0.5000	0.5000	0.2812	0.20884
C	1*a*	0.0000	0.0000	0.0000	0.31818

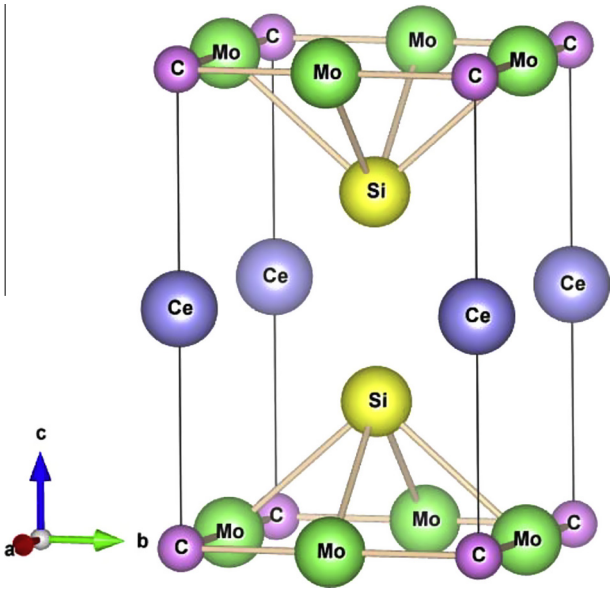

Fig. 2. Tetragonal crystal structure of $CeMo_2Si_2C$ (space group *P4/mmm*). The atomic coordinates are listed in Table 1.

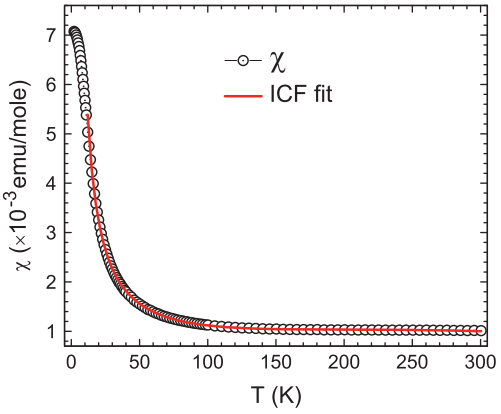

Fig. 3. Temperature dependence of the magnetic susceptibility of $CeMo_2Si_2C$ at 5 T. The solid red line through the magnetic susceptibility data shows a fit to the two-level ionic interconfiguration fluctuations (ICF) model in the temperature range 10–300 K. (For interpretation of the references to color in this figure legend, the reader is referred to the web version of this article.)

curves has been observed and are typical for Ce-based valence fluctuating compounds [24–27]. Sometimes the magnetic susceptibility does show a curie tail at lower temperatures in valence fluctuating systems for instance in $Ce_2Co_3Ge_5$ [24], $Ce_2Ni_3Si_5$ [27], and $CeNi_2B_2C$ [28]. which arises due to free Ce^{3+} magnetic impurity ions.

The dc magnetic susceptibility for a valence fluctuating system can be described with the two level ionic interconfiguration fluctuation (ICF) model. The theory of ICF was first proposed by Hirst [30] and latter Sales and Wohlleben developed it further to explain the valence fluctuating behavior observed in few Yb-based compounds [31]. According to the ICF model [32], the temperature dependence of the susceptibility is given by

$$\chi(T) = \left(\frac{N}{3k_B}\right)\left[\frac{\mu_n^2 v(T) + \mu_{n-1}^2\{1 - v(T)\}}{T^*}\right] \quad (1)$$

with

$$v(T) = \frac{2J_n + 1}{(2J_n + 1) + (2J_{n-1} + 1)exp(-E_{ex}/K_B T^*)} \quad (2)$$

and

$$T^* = \left[T^2 + T_{sf}^2\right]^{1/2} \quad (3)$$

where μ_n and μ_{n-1} are the effective moments in $4f^n$ and $4f^{(n-1)}$ states, and $(2J_n + 1)$ and $(2J_{n-1} + 1)$ are the degeneracies of the corresponding energy states E_n and E_{n-1}. Here E_{ex} is interconfigurational excitation energy which is equals to $(E_n) - (E_{n-1})$ and T_{sf} is the spin fluctuation temperature associated with the valence fluctuation. In order to take care of the contribution of Ce^{3+} ions which belong to the impurity phases present in $CeMo_2Si_2C$, we have added the term $\chi_{imp} = n * C/(T - \theta)$ to the magnetic susceptibility. Thus the final equation is

$$\chi(T) = (1 - n)\left(\frac{N}{3k_B}\right)\left[\frac{(2.54\ \mu_B)^2\{1 - v(T)\}}{T^*}\right] + n\frac{C}{T - \theta} + \chi_0 \quad (4)$$

with

$$v(T) = \frac{1}{1 + 6exp(-E_{ex}/K_B T^*)} \quad (5)$$

where χ_0 is temperature independent term and n is the fraction of stable Ce^{3+} ions. Here we have taken Ce^{4+} ($J = 0$ and $\mu = 0\ \mu_B$) state as ground state and Ce^{3+} ($J = \frac{5}{2}$ and $\mu = 2.54\ \mu_B$) as an excited state. The solid line through the magnetic susceptibility data in Fig. 3 is the fit to the Eq. (4). The values of parameters obtained from the least square fits are $n = 0.06, E_{ex} = 677 \pm 12$ K, $T_{sf} = 205 \pm 3$ K, $\theta = 1.9$ K and $\chi_0 = -1.67 \times 10^{-4}$ emu/mole. The values of E_{ex} and T_{sf} are in the range of typical values found for the valence-fluctuating system $Ce_2Rh_3Si_5$ ($E_{ex} = 845$ K and $T_{sf} = 129$ K) [22].

Furthermore, to understand the intrinsic behavior of the susceptibility for the sample, i.e. $\chi(T)$ without the contribution from Ce^{3+} impurity phase, we have subtracted the magnetic impurity contribution from the measured susceptibility data. The susceptibility data were first fitted to the equation $\chi(T) = \chi_0 + n * C/(T - \theta)$ in the temperature range 15–80 K where the dominant magnetic contribution is coming from Ce^{3+} magnetic impurity phase (see Fig. 4). The parameters obtained from the least square fit, $n = 0.06$ and $\theta = 2.32$ K are nearly same as found in the impurity part of ICF fitting discussed earlier. In next step, the impurity part $\chi_{imp} = n * C/(T - \theta)$ was subtracted from the measured $\chi(T)$ in the temperature range 10–300 K. The resulted (after subtraction) susceptibility $\chi - \chi_{imp}$ posses a broad maximum which is a characteristic feature of a valence fluctuating system [22,33] (see inset of Fig. 4). The $\chi - \chi_{imp}$ data were fitted to the following ICF equation

$$\chi(T) = (1 - n)\left(\frac{N}{3k_B}\right)\left[\frac{(2.54\ \mu_B)^2\{1 - v(T)\}}{T^*}\right] + \chi_0 \quad (6)$$

where the impurity concentration n is kept fixed at 0.06. The fit to the data yields the values $E_{ex} = 701 \pm 4$ K, $T_{sf} = 217 \pm 1$ K and $\chi_0 = -1.24 \times 10^{-4}$ emu/mole, which are close to the values obtained from the ICF fitting earlier above.

Even though the valence fluctuating systems are not expected to order magnetically, the magnetic susceptibility measured under low magnetic fields exhibit sharp increase below 8 K (Fig. 5). However, the low value of magnetization at 5 K (~0.003 μ_B/Ce at 0.01 T) and the absence of any anomaly in the specific heat data suggest that this low temperature magnetic susceptibility anomaly is not intrinsic and arises from small amount of impurity phase. The field dependence indicate this impurity phase to be ferromagnetic. Therefore it is likely a small amount of $CeSi_{2-x}$ [34].

The specific heat $C(T)$ of $CeMo_2Si_2C$ measured under zero applied magnetic field is presented in Fig. 6 in the temperature range 1.8–35 K. The specific heat exhibits no anomaly in this temperature range down to 1.8 K and hence confirms the absence of

Table 2
Powder pattern of $CeMo_2Si_2C$, the calculated values are obtained from the Rietveld refinement of powder X-ray diffraction data and the observed values are the experimental values.

2θ	hkl	d_{hkl}	I_{cal}	I_{obs}	2θ	hkl	d_{hkl}	I_{cal}	I_{obs}
16.477	001	5.375545	185.0	189.1	66.541	300	1.404098	18.9	20.8
21.073	100	4.212293	437.3	464.0	68.722	203	1.36476	36.8	38.2
26.867	101	3.315601	654.9	643.1	69.083	301	1.358519	55.7	53.7
29.975	110	2.978541	4	3.7	69.944	004	1.343886	108.6	116
33.307	002	2.687773	550.5	559	70.658	310	1.332044	1.2	1.5
34.394	111	2.605331	2479.7	2472.6	72.5	222	1.302666	202.5	202.3
39.749	102	2.265809	673.8	667.4	72.782	213	1.298317	130.9	130.8
42.905	200	2.106147	1482.2	1473.1	73.133	311	1.29294	663.9	687.8
45.414	112	1.995443	121.4	128.8	73.974	104	1.280306	27.3	25.8
46.258	201	1.961003	54.4	51.4	76.478	302	1.244513	107.8	110.1
48.271	210	1.883795	81.1	89.2	77.925	114	1.224973	1.1	1.1
50.92	003	1.791848	21.8	21	80.39	312	1.193512	54.4	57.8
51.352	211	1.777793	214.5	224.7	82.497	320	1.16828	16.6	19.1
55.374	202	1.657801	561.4	516.3	84.527	223	1.145326	17.9	20
55.7	103	1.648865	151.9	159.9	84.865	321	1.141629	53.2	59.3
59.911	212	1.54263	364.8	355.8	85.674	204	1.132904	271	264.1
60.222	113	1.535422	364.4	375.3	88.367	303	1.1052	48.3	48.3
62.292	220	1.489271	343.6	376.6	89.51	214	1.094027	32.4	34.6
64.919	221	1.43521	14.4	16.4					

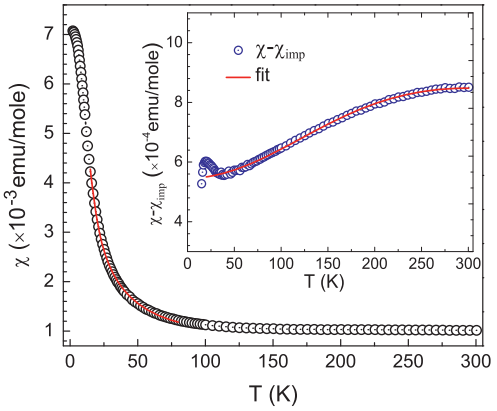

Fig. 4. Temperature dependence of the magnetic susceptibility of $CeMo_2Si_2C$ at 5 T. The solid line through the magnetic susceptibility data in the temperature range 15–80 K shows a fit to the equation $\chi(T) = \chi_0 + n * C/(T-\theta)$. The blue circles in the inset represent the susceptibility data obtained after subtracting the extrapolated impurity component from the measured susceptibility data in the temperaure range 10–300 K and the solid line through the data points represents an ICF fit as discussed in the text. (For interpretation of the references to colour in this figure legend, the reader is referred to the web version of this article.)

magnetic ordering in $CeMo_2Si_2C$. We could fit the low temperature specific heat data below 12 K to the equation

$$C(T) = \gamma T + \beta T^3 \tag{7}$$

where γT is the electronic contribution to the specific heat, βT^3 is the phononic contribution to the specific heat (inset of the Fig. 6). The fit to the data yields the value of $\gamma = 23.4$ mJ/mol K^2 and $\beta = 1.6 \times 10^{-4}$ J/mol K^4. This gamma value is at the lower border of the range expected for valence fluctuating Ce system, but comparable to the value found, e.g. in $CeRu_2$ (γ = 23 mJ/mol K^2) [35], $Ce_2Co_3Ge_5$ (γ=17 mJ/mol K^2) [24] and $CeRu_3Si_2$ (γ = 39 mJ/mol K^2) [29]. The Debye temperature Θ_D for $CeMo_2Si_2C$ was estimated from β using the relation [36]

$$\Theta_D = \left(\frac{12\pi^4 nR}{5\beta}\right)^{1/3} \tag{8}$$

where R is molar gas constant and $n = 6$ is the number of atoms per formula unit (f.u.). Form this, we obtain Debye temperature $\Theta_D = 417$ K for $CeMo_2Si_2C$.

The temperature dependence of electrical resistivity $\rho(T)$ of $CeMo_2Si_2C$ is shown in Fig. 7. The electrical resistivity data exhibit metallic behavior with residual resistivity, $\rho_0 \sim 12.7$ μΩ cm at 2 K.

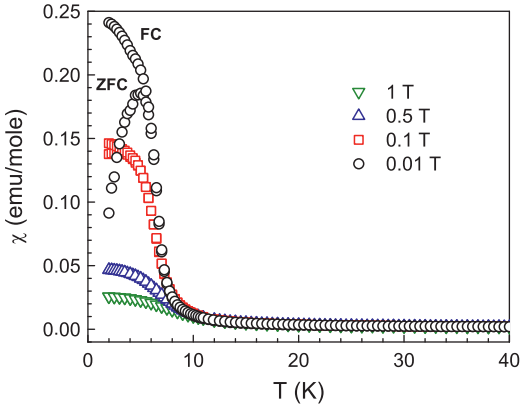

Fig. 5. The temperature dependence of zero field-cooled (ZFC) and field-cooled (FC) dc magnetic susceptibility in the temperature range 2–40 K measured under various applied magnetic fields.

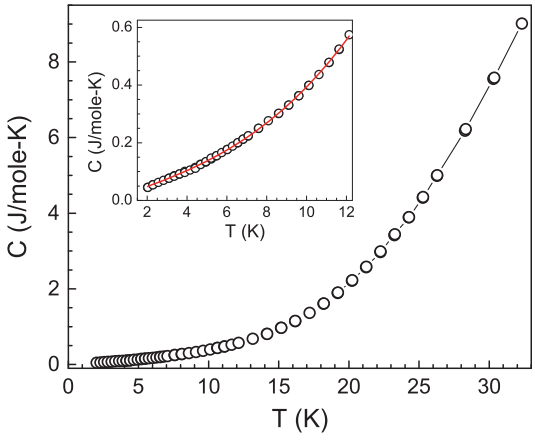

Fig. 6. Temperature dependence of the specific heat data, $C(T)$ of $CeMo_2Si_2C$ measured in zero field in the temperature range (1.8–35 K). The solid line through the specific heat data in the inset shows the fit to the equation $C(T) = \gamma T + \beta T^3$.

The large value of residual resistivity ratio ($RRR = \rho_{300\,K}/\rho_{2\,K}$) ~ 9 indicates good crystallinity of our sample. We do not observe any prominent anomaly in the resistivity data and the data fit well to the following equation in the low temperature range 10–35 K, i.e.

$$\rho(T) = \rho_0 + AT^2 \quad (9)$$

The fitting yield the parameters $\rho_0 \sim 12.3\ \mu\Omega\,cm$ for the residual resistivity and the coefficient $A = 2.57 \times 10^{-3}\ \mu\Omega\,cm\,K^{-2}$. Thus, the electrical resistivity of $CeMo_2Si_2C$ exhibits the Fermi liquid behavior as usually observed for Ce-based valence fluctuating systems [37]. Within the Fermi liquid theory the A coefficient is related to γ^2. Kadowaki and Woods found that in heavy fermion systems and valence fluctuating systems the ratio A/γ^2 is of the order of $1 \times 10^{-5}\ \mu\Omega\,cm\,(mol\,K/mJ)^2$ [38]. Later on Tsujii et al. [39]. suggested this ratio to scale with $2/N(N-1)$ where N is the degeneracy of the orbital state of the f element. For an intermediate valent Ce system $N = 6$ gives $A/\gamma^2 = 6.7 \times 10^{-7}\ \mu\Omega\,cm\,(mol\,K/mJ)^2$. For $CeMo_2Si_2C$ our experimental data result in $A/\gamma^2 = 0.5 \times 10^{-5}\ \mu\Omega\,cm\,(mol\,K/mJ)^2$, just the original Kadowaki Woods value. Furthermore, in a Fermi liquid one expect a T-independent susceptibility χ_{FL} at low temperatures with a value scaling with γ too. This is expressed in the Wilson Sommerfeld ratio i.e.

$$R_W = \frac{\pi^2 k_B^2 \chi_{FL}}{\gamma \mu_{eff}^2} \quad (10)$$

which is expected to be close to one. Taking the low temperature value of $\chi_{FL} \approx 5.6 \times 10^{-4}$ emu/mole from the impurity corrected $\chi(T)$ shown in the inset of Fig. 4, $\gamma = 23.4\ mJ/mol\,K^2$ as determined above, and $\mu_{eff} = 2.54\ \mu_B$ as expected for the free Ce^{3+} moment we get $R_W = 0.81$, while taking $\mu_{eff} = 1.73\ \mu_B$ as for a free conduction electron, one get $R_W = 1.7$. Thus, low T susceptibility, specific heat and resistivity data fulfill Fermi liquid expectations.

The Ce–L_{III}-edge X-ray absorption spectrum of $CeMo_2Si_2C$ taken at room temperature is presented in Fig. 8. To analyze the spectrum in detail two Gaussian functions were taken into consideration which represents the $4f^1$ and $4f^0$ configuration. Additionally, two arc tan function was added to provide the relative weight of the two electron configurations. The larger peak at 5724 eV corresponds to the $4f^1$ configuration and the smaller peak at 5734 eV corresponds to the $4f^0$ configuration. The Ce–L_{III} clearly indicates that the Ce ions in this compound are in valence fluctuating state. Moreover, the average formal L_{III} valence of Ce can be obtained from the intensity ratio of the two Gaussian peaks using the equation $\langle\tilde{\nu}\rangle = 3 + I_1/(I_1 + I_2)$. Hence we get the value of average formal L_{III} valence of Ce atoms in $CeMo_2Si_2C$ as $\langle\tilde{\nu}\rangle = 3.14$ at room temperature. This value is less than the value (~3.4) obtained for a tetravalent CeO_2 [40]. Similar values of mean formal L_{III} valence of Ce ions have also been reported for other valence fluctuating compounds, for example, $CeRhSi_2$ ($\langle\tilde{\nu}\rangle = 3.15$), $Ce_2Rh_3Si_5$($\langle\tilde{\nu}\rangle = 3.18$) [22] and $CeNi_2B_2C$ ($\langle\tilde{\nu}\rangle = 3.18$) [28] at room temperature.

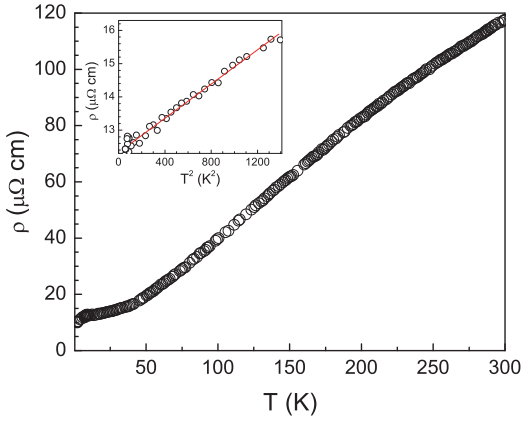

Fig. 7. Temperature dependence of electrical resistivity data, $\rho(T)$ of $CeMo_2Si_2C$ as a function of temperature. The solid line in the inset shows the fit to the equation $\rho(T) = \rho_0 + AT^2$.

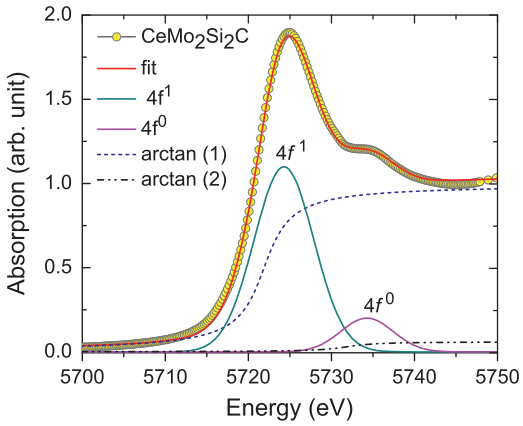

Fig. 8. Ce–L_{III}-edge X-ray absorption of $CeMo_2Si_2C$ at 300 K. The solid black line through data points shows the least square fit. The contributions due to $4f^1$ and $4f^0$ configurations are represented by the solid Gaussian lines, while the dashed line represents the arctan functions.

3.2. Band structure calculations

In order to gain some information on the electronic state, electronic structure calculations were performed for the compound using two different approaches, i.e., with FPLO and full potential LAPW method. Both the methods give very similar results and therefore only those obtained by using the FLAPW method are discussed here. Because of the strong correlations in the (4*f*) shell, the density functional approach is not able to treat the (4*f*)-electrons of Ce accurately. In contrast non-*f* valence states are usually only weakly affected by these correlations, except close to the Fermi level where hybridization with *f*-states becomes relevant. Therefore, such a calculation allows insight into the non-*f* valence states and gives some information on the states which are hybridized with the Ce (4*f*) states at the Fermi level. In this method the unit cell is divided into non-overlapping muffin-tin spheres centered at the atomic sites and an interstitial region. The muffin-tin radii were chosen to be of 2.5 a.u. for Ce, 2.1 a.u. for Mo, 2.2 a.u. for Si and 1.86 a.u. for C. The set of plane-wave expansion K_{MAX} was determined as $R_{MT} \times K_{MAX}$ equal to 7 and K mesh used was $13 \times 13 \times 10$. We have performed the calculations with and without spin polarization. Notably the self-consistent results for magnetic solutions were nearly the same as those for non-magnetic ones because the spin polarized calculation resulted in a non-magnetic state. Total and local magnetic moments were approximately zero ($\sim 10^{-5}\ \mu_B$/Ce) in the spin polarized calculations.Fig. 9 shows the total and partial Density of States (DOSs) for $CeMo_2Si_2C$, calculated within the GGA and GGA + U (U = 6 eV) approximations. To describe in detail, here we divide the total DOS into four main parts.

1. The peak located below −16 eV is due to Ce 5*p* electronic state. It is remarkable that the GGA + U peak is shifted towards higher binding energy by 1 eV with respect to GGA.
2. The sub-band situated between −12 eV and −6 eV, is formed mainly by Si 3*s* and C 2*s* states.
3. The third part, which is located between the −6 and −2 eV contains strongly hybridized Mo 4*d* , Si 3*p* and C 2*p* states. Hybridized states of Ce 4*d* and C 2*p* are observed as well just below the Fermi level (see the partial density of states of Fig. 9).

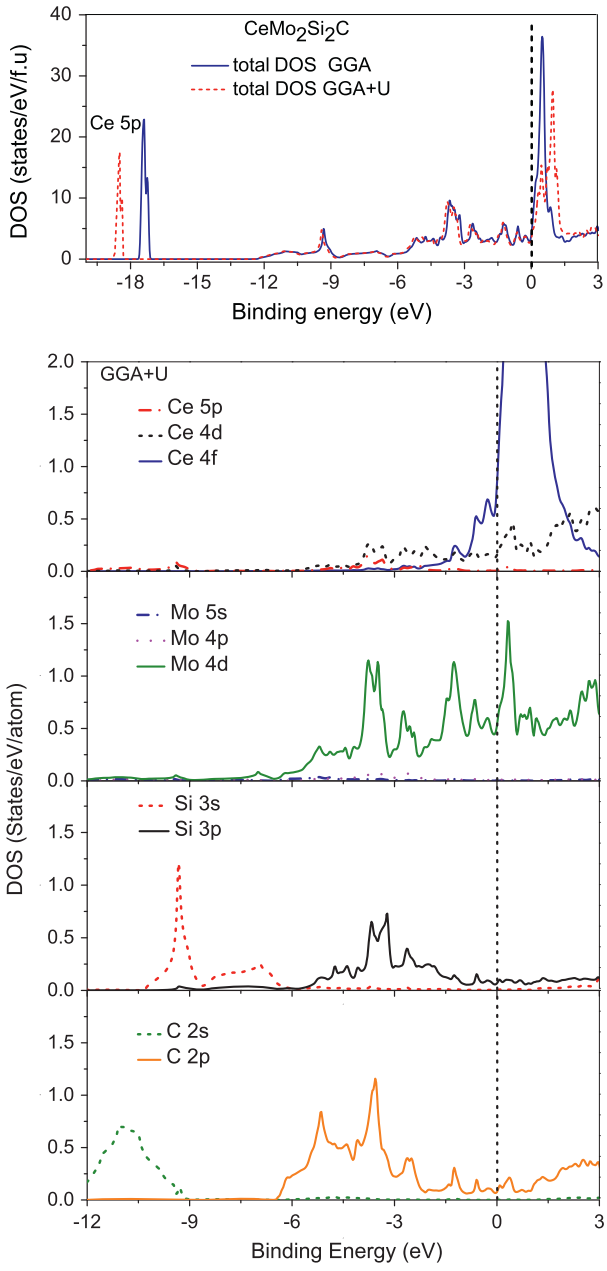

Fig. 9. Total (upper panel) and partial densities of states (bottom panels) for $CeMo_2Si_2C$. Here the Fermi level (E_F) corresponds to zero binding energy.

4. The bottom of the conduction band or at the Fermi level, the main contribution to the DOS is provided by Ce (4*f*) and Mo 4*d* electronic states. Hybridization between Ce 4*f* and Mo 4*d* states are observed near the Fermi level. In case of GGA + U the main peak (Ce (4*f*)) is broadened and slightly shifted towards right side above the Fermi level in comparison to GGA and consequently reduced the occupancy of Ce (4*f*) electrons at the Fermi level.

It should be noted that at the Fermi level a small contribution to the total DOS come from Ce 5*d*, Si 3*p* and C 2*p* states as well. The orbital occupancy of electrons inside the atomic sphere of the Ce atom is calculated by the GGA approach as $6s^{1.98}\ 5d^{0.64}\ 4f^{0.94}$ and by GGA + U calculation as $6s^{1.99}\ 5d^{0.85}\ 4f^{0.64}$. Thus the *f*-count in these calculations is slightly (GGA) or far (GGA + U) below 1. Comparison with the L_{III} result shows that GGA overestimate the *f* count while GGA + U provides more realistic value of *f* electron count.

Table 3
Total densities of states $N[E_F]$ (in states/eV/f.u) and partial densities of states (in states/eV/atom) at the Fermi level, the calculated Sommerfeld coefficient γ_0 (in mJ/mol $K_{(2)}$ and molar Pauli paramagnetic susceptibility χ_{FL} (in 10^{-4} emu/mol).

Method	Total $N[E_F]$	γ_0	χ_{FL}	Ce-(4*f*)	Mo-4*d*
GGA	3.86	9.10	1.24	1.47	0.52
GGA + U	3.16	7.45	1.01	0.77	0.52

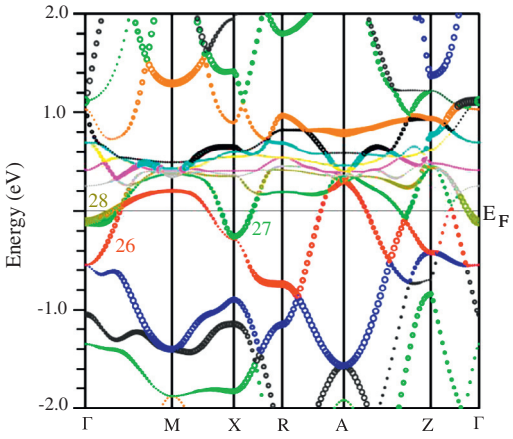

Fig. 10. Band structure of $CeMo_2Si_2C$ along the symmetry lines of the Primitive tetragonal BZ. Mo 4*d* contribution to the bands is represented by the larger circles. Different colors of the bands are used just to guide the eyes. (For interpretation of the references to color in this figure legend, the reader is referred to the web version of this article.)

Based on the DOS at the Fermi level here we obtained the Sommerfeld coefficients γ_0 and the Pauli paramagnetic susceptibility χ_{FL} as calculated under the assumption of free electron model, $\gamma_0 = (\pi^2/3)N[E_F]K_B^2$ and $\chi_{FL} = \mu_B^2 N[E_F]$, where $N[E_F]$ is the electron density of states at the Fermi level. All the calculated values are listed in Table 3. The calculated γ_0 and χ_{FL} values are a factor of about 3 and 6, respectively, below the experimental values. This difference can be very simply attributed to the strong renormalization connected with the valence fluctuations.

The band structure along various symmetry directions calculated within the GGA is shown in Fig. 10. The band structure close to the Fermi level is mainly composed of three bands (bands 26, 27 and 28) which are crossing E_F. The fat part (bigger circles) of the bands represent the contribution from Mo 4*d* states which are considerably hybridized with the Ce (4*f*) bands near E_F. Two electron like bands (bands 27 and 28) cut by the Fermi level at Γ and *X* points and a highly dispersed hole like band (band 26) crosses the Fermi level at *M* and *A* points. The strong dispersion along Γ–*Z* shows that this compound, despite having a quasi 2D structure, has a true 3D electronic structure. Interesting features are observed between Γ–*Z* and *A*–*Z* as the sharp tip of the bottom of the conduction band touches the sharp tip of the top of the valence band.

4. Conclusion

To summarize, our comprehensive studies of physical properties of $CeMo_2Si_2C$ by $\chi(T), C(T), \rho(T)$, and XAS measurements reveal the valence fluctuating state of Ce in $CeMo_2Si_2C$. The compound crystallizes in the $CeCr_2Si_2C$-type layered tetragonal structure (space group *P4/mmm*). The value of magnetic susceptibility is very low and almost independent of temperature except a curie tail at lower temperature (as observed in many valence fluctuating compounds) which arises due to a small amount (~6%) of an impurity

Ce^{3+} phase present in the sample. An ICF analysis of $\chi(T)$ result in a fluctuation temperature T_{sf} = 205 ± 3 K and an interconfigurational excitation energy E_{ex} = 677 ± 12 K. The temperature dependence of specific heat at zero magnetic field does not show any anomaly throughout the temperature range and hence confirms the absence of any magnetic ordering down to 2 K. The Sommerfeld coefficient obtained from the specific heat data γ = 23.4 mJ/mol K^2 is relatively low for a valence fluctuating compound which indicates a strong hybridization of Ce (4*f*) states with the conduction states at the Fermi level. The electrical resistivity exhibits a metallic behavior with a T^2 dependence in the low temperature range indicating the Fermi liquid behavior as observed for many Ce-based valence fluctuating systems. XAS studies indicate an average formal L_{III} valence $\langle\tilde{\nu}\rangle = 3.14$ hence gives a direct evidence for valence fluctuations. Nevertheless, this value is less than that obtained for a tetravalent CeO_2 ($\langle\tilde{\nu}\rangle \simeq 3.4$). The density functional calculations show strong dispersions along all direction evidencing a 3D electronic structure despite the quasi 2D chemical structure. Strong hybridization is found between Mo 4*d*, Si 3*p* and C 2*p* states, and between Ce 4*d* and C 2*p* states at lower binding energies below the Fermi level. The bands at the Fermi level bear a large Mo 4*d* character and provide the states which are hybridized with the Ce (4*f*) states.

Acknowledgements

This work has been supported by the Council of Scientific and Industrial Research, New Delhi (Grant No. 80(0080)/12/EMR-II). We acknowledge Dr. Edmund Walter (beam-line scientist) for technical support.

References

[1] D. Wohlleben, B. Wittershagen, Adv. Phys. 34 (1985) 403.
[2] G.R. Stewart, Rev. Mod. Phys. 56 (1984) 755.
[3] N.B. Brandt, V.V. Moshchalkov, Adv. Phys. 33 (1984) 373.
[4] P. Gegenwart, Q. Si, F. Steglich, Nat. Phys. 4 (2008) 186.
[5] S. Doniach, Physica B 91 (1977) 231.
[6] C. Lacroix, M. Cyrot, Phys. Rev. B 20 (1979) 1969.
[7] F. Steglich, J. Aarts, C.D. Bredl, W. Lieke, D. Meschede, W. Franz, H. Schäfer, Phys. Rev. Lett. 43 (1979) 25.
[8] H.Q. Yuan, F.M. Grosche, M. Deppe, C. Geibel, G. Sparn, F. Steglich, Science 302 (5653) (2003) 2104.
[9] E. Lengyel, M. Nicklas, H.S. Jeevan, C. Geibel, F. Steglich, Phys. Rev. Lett. 107 (2011) 057001.
[10] S. Nakatsuji, K. Kuga, Y. Machida, T. Tayama, T. Sakakibara, Y. Karaki, H. Ishimoto, S. Yonezawa, Y. Maeno, E. Pearson, G.G. Lonzarich, L. Balicas, H. Lee, Z. Fisk, Nat. Phys. 4 (2008) 603.
[11] Yosuke Matsumoto, Kentaro Kuga, Takahiro Tomita, Yoshitomo Karaki, Satoru Nakatsuji, Phys. Rev. B 84 (2011) 125126.
[12] Matsumoto Yosuke, Nakatsuji Satoru, Kuga Kentaro, Science 331 (2011) 6015–6316.
[13] E. Dashjav, W. Schnelle, F.R. Wagner, G. Kreiner, R. Kniep, Z. Kristallogr. NCS 221 (2006) 267.
[14] V. Klosek, A. Vernière, B. Malaman, J. Tobola, S. Kaprzyk, Phys. Rev. B 78 (2008) 104419.
[15] Chengchun Tang, Shoushan Fan, Meijian Zhu, J. Allyos Comp. 299 (2000) 1.
[16] K. Mukherjee, K.K. Iyer, E.V. Sampathkumaran, J. Phys.: Condens. Matter 22 (2010) 295603.
[17] Athena, Artemis, J. Synchrotron Rad. 12 (2005) 537.
[18] K. Koepernik, H. Eschrig, Phys. Rev. B 59 (1999) 1743.
[19] P. Blaha, K. Schwarz, G. Madsen, An Augmented Plane Wave Plus Local Orbitals Program for Calculating Crystal Properties, Vienna University of Technology, Vienna, 2001.
[20] V.I. Anisimov, O. Gunnarsson, Phys. Rev. B 43 (1991) 7570.
[21] J.P. Perdew, K. Burke, M. Ernzerhof, Phys. Rev. Lett. 77 (1996) 3865.
[22] D. Kaczorowski, A.P. Pikul, U. Burkhardt, M. Schmidt, A. Ślebarski, A. Szajek, M. Werwiński, Yu Grin, J. Phys.: Condens. Matter 22 (2010) 215601.
[23] J. Rodríguez-Carvajal, Physica B 192 (1993) 55;
Program Fullprof, LLB-JRC, Laboratoire Léon Brillouin, CEA-Saclay, France, 1996.
[24] S. Layek, V.K. Anand, Z. Hossain, J. Magn. Magn. Mater 321 (2009) 3447.
[25] D.P. Rojas, L.C.J. Pereira, P. Salamakha, E.B. Lopes, J.C. Waerenborgh, L.M. da Silva, F.G. Gandra, J. Alloys Comp. 391 (2005) L5.
[26] A. Kowalczyk, M. Pugaczowa-Michalska, T. Toliński, Phys. Status Solidi B 242 (2005) 433.
[27] C. Mazumdar, R. Nagarajan, S.K. Dhar, L.C. Gupta, R. Vijayaraghavan, B.D. Padalia, Phys. Rev. B 46 (1992) 9009.
[28] E. Alleno, Z. Hossain, C. Godart, R. Nagarajan, L.C. Gupta, Phys. Rev. B 52 (1995) 7428.
[29] U. Rauchschwalbe, W. Lieke, F. Steglich, C. Godart, L.C. Gupta, R.D. Parks, Phys. Rev. B 30 (1984) 444.
[30] L.L. Hirst, Phys. Kondens. Mater. 11 (1970) 255.
[31] B.C. Sales, D.K. Wohlleben, Phys. Rev. Lett. 35 (1975) 1240.
[32] W. Franz, F. Steglich, W. Zell, D. Wohlleben, F. Pobell, Phys. Rev. Lett. 45 (1980) 64.
[33] S.K. Malik, D.T. Adroja, Phys. Rev. B. 43 (1991) 6277. R.
[34] H. Yashima, H. Mori, T. Satoh, K. Kohn, Solid State Commun. 43 (1982) 193.
[35] J.W. Allen, S.-J. Oh, I. Lindau, M.B. Maple, J.F. Suassuna, S.B. Hagström, Phys. Rev. B 26 (1982) 445.
[36] C. Kittel, Introduction to Solid State Physics, eighth ed., Wiley, New York, 2005.
[37] K. Andres, J.E. Graebner, H.R. Ott, Phys. Rev. Lett. 35 (1975) 1779.
[38] K. Kadowaki, S.B. Woods, Solid State Commun. 58 (1986) 507.
[39] N. Tsujii, H. Kontani, K. Yoshimura, Phys. Rev. Lett. 94 (2005) 057201.
[40] E.E. Vainshtein, S.M. Bloklin, Y.B. Paderno, Sov. Phys. Solid State 6 (1965) 2318.